RSC Advances

PAPER

Cite this: *RSC Adv.*, 2016, **6**, 55233

Effect of preparation method on performance of Cu–Fe/SiO_2 catalysts for higher alcohols synthesis from syngas

Chao Sun, Dongsen Mao,* Lupeng Han and Jun Yu

Received 21st March 2016
Accepted 2nd June 2016

DOI: 10.1039/c6ra07366b

www.rsc.org/advances

Five Cu–Fe/SiO_2 catalysts were prepared by deposition–precipitation, solid state impregnation, solid-state chemical reaction, citric acid combustion, and ultrasound-assisted wet impregnation, and their physicochemical and catalytic properties for higher alcohols synthesis were investigated. The results showed that the Cu–Fe/SiO_2 catalyst prepared by ultrasound-assisted impregnation had a higher dispersion and reducibility of active metal oxides, and the largest S_{Cu}, which increased the amount of adsorbed CO and the ability for CO dissociation. As a result, the CO conversion and space time yield of total alcohols of the catalyst reached 14.04% and 104.3 g kg^{-1} h^{-1}, respectively, which were better than the other catalysts.

1. Introduction

Higher alcohols synthesis (HAS) from coal, natural gas or lignocellulosic biomass *via* synthesis gas (syngas, CO + H_2) has attracted increasing attention due to their potential application as liquid fuel, additives for gasoline, hydrogen carriers for fuel cells, and intermediates for chemicals.[1–4] Several catalytic systems have been studied extensively so far for HAS such as noble Rh-based catalysts, modified methanol synthesis catalysts, modified Fischer–Tropsch (F–T) synthesis catalysts and Mo-based sulphur tolerance catalysts.[2,4–6] Noble Rh-based catalysts have little attraction for commercial utilization due to the high cost and limited availability in large scale production.[7–10] Among the non-noble metal-based catalysts, cobalt modified Cu-based catalyst has been considered as one of the most promising catalysts,[3,11,12] however, the low total alcohol selectivity and poor stability limit its large scale industrial application.[13,14]

In recent years, Fe modified Cu-based catalysts were also investigated by many researchers.[11,13–27] For example, Lin *et al.* reported that the catalytic performance of zinc and manganese doubly promoted Cu–Fe catalyst was superior to that of the zinc or manganese singly promoted Cu–Fe catalyst, which was attributed to the synergistic effect between zinc and manganese on the Cu–Fe catalyst.[14] Zhang *et al.* found that plasma-promoted Cu–Fe/SiO_2 catalyst possessed higher CO conversion, total alcohol selectivity and selectivity of $C_{2+}OH$ in alcohols than those of conventional sample for HAS.[16] Ding *et al.* reported that Cu–Fe catalyst supported on the bimodal pore SiO_2 exhibited higher selectivity of $C_{2+}OH$ in total alcohols compared with that of catalyst supported on larger and smaller pore SiO_2, which was contributed to the well dispersion of active metals and high diffusion of products in the bimodal structures.[18] Although some promising results have been obtained on the Fe modified Cu-based catalyst, there are still several problems to be solved, such as low selectivity to alcohols, high hydrocarbons selectivity and products with plenty of water.[18,20,21] Thus, how to further improve the activity and selectivity of Cu–Fe based catalyst for HAS remains the key of research.[14,18]

In the present study, for the purpose of improving the catalytic performance of Cu–Fe/SiO_2 catalysts for HAS, they were prepared by five methods including deposition–precipitation, solid-state impregnation, solid-state chemical reaction, citric acid combustion, and ultrasound-assisted wet impregnation. In order to clearly elucidate the influence of preparation methods, the physicochemical properties of the catalysts were characterized by X-ray diffraction (XRD), N_2 adsorption–desorption, Fourier transform infrared (FT-IR) spectroscopy, H_2 temperature-programmed reduction (H_2-TPR), X-ray photoelectron spectra (XPS), temperature-programmed desorption of adsorbed CO (CO-TPD), and N_2O reactive frontal chromatography.

2. Experimental

2.1. Materials and catalyst preparation

A commercial silica gel (Qingdao Haiyang Chemicals Company, China) was first dried at 110 °C overnight in an electric oven, and then used as the support in this study. The Cu–Fe/SiO_2 catalysts were prepared by five different methods, *viz.*, ultrasound-assisted wet impregnation (WI), deposition–

Research Institute of Applied Catalysis, School of Chemical and Environmental Engineering, Shanghai Institute of Technology, Shanghai 201418, P.R. China. E-mail: dsmao@sit.edu.cn; Fax: +86 21 6087 3625; Tel: +86 21 6087 3625

precipitation (DP), solid-state impregnation (SI), solid-state chemical reaction (SR), and citric acid combustion (CC). Both the Cu and Fe loadings of the catalysts were 10% mole fraction relative to support SiO_2. The $Cu(NO_3)_2 \cdot 3H_2O$, $Fe(NO_3)_3 \cdot 9H_2O$, NaOH, oxalic acid, and citric acid were of analytical purity and purchased from Chinese Sinopharm Chemical Reagent Co., Ltd., China.

Preparation of Cu–Fe/SiO_2 by ultrasound-assisted wet impregnation method. For the preparation of Cu–Fe/SiO_2(WI), appropriate amounts of $Cu(NO_3)_2 \cdot 3H_2O$ and $Fe(NO_3)_3 \cdot 9H_2O$ were dissolved in 4 mL of distilled water. To this solution, the SiO_2 was soaked in the solution under ultrasonic irradiation. Sonication was carried out on a KQ-250E instrument (Kunshang Ultrasonic Instrument Co., Ltd., Jiangsu, China) with power of 250 W at 40 kHz for 30 min. Then this solution was slowly evaporated under ambient atmosphere, after that the impregnated sample was dried at 110 °C for 10 h and then calcined in static air at 350 °C for 4 h.

Preparation of Cu–Fe/SiO_2 by deposition–precipitation method. For the preparation of Cu–Fe/SiO_2(DP), appropriate amounts of $Cu(NO_3)_2 \cdot 3H_2O$ and $Fe(NO_3)_3 \cdot 9H_2O$ were dissolved in 10 mL distilled water. Required amount of SiO_2 was dispersed in this solution and mixed thoroughly with a magnetic stirrer. To this, an aqueous NaOH solution (0.1 M) was added drop wise with continuous stirring at ambient temperature, till complete precipitation (pH = 7–9) was achieved. Then, the suspension was aged for 3 h in water bath at 70 °C. Subsequently, the precipitate was filtered and washed several times with distilled water to remove the sodium ions and then dried in air at 110 °C overnight. The dried sample was calcined at 350 °C in static air for 4 h to obtain the final catalyst.

Preparation of Cu–Fe/SiO_2 by solid-state impregnation. For the preparation of Cu–Fe/SiO_2(SI), appropriate amounts of $Cu(NO_3)_2 \cdot 3H_2O$, $Fe(NO_3)_3 \cdot 9H_2O$ and SiO_2 were mixed and ground for 30 min at room temperature. After that the mixture was dried in air at 110 °C overnight, and then the dried sample was calcined at 350 °C for 4 h in static air to obtain the final catalyst.

Preparation of Cu–Fe/SiO_2 by solid-state chemical reaction. For the preparation of Cu–Fe/SiO_2(SR), appropriate amounts of $Cu(NO_3)_2 \cdot 3H_2O$, $Fe(NO_3)_3 \cdot 9H_2O$, SiO_2, and oxalic acid (molar ratio relative to active metals was 1.5 : 1) were mixed and ground for 30 min at room temperature. After that the sample was dried at 110 °C overnight in an electric oven, and then the dried sample was calcined at 350 °C for 4 h in static air.

Preparation of Cu–Fe/SiO_2 by citric acid combustion. For the preparation of Cu–Fe/SiO_2(CC), appropriate amounts of $Cu(NO_3)_2 \cdot 3H_2O$ and $Fe(NO_3)_3 \cdot 9H_2O$ were dissolved in 10 mL distilled water, and the SiO_2 was dispersed in this solution. The prepared citric acid aqueous solution was added drop wise with continuous stirring at ambient temperature, till the molar ratio of citric acid to active metals of Cu and Fe was 1.2. Then the sample was treated under ultrasonic irradiation to obtain orange gel. It was evaporated at 350 °C in a muffle roaster till it combusted; after that the sample was further calcined at 350 °C for 4 h to yield the final catalyst.

2.2. Catalyst testing

CO hydrogenation reaction was carried out in a fixed-bed micro-reactor with length of 350 mm and internal diameter of 5 mm.[26] The fresh catalyst (0.3 g) was loaded between quartz wool and axially centred in the reactor tube, with the temperature monitored by a thermocouple close to the catalyst bed. Prior to reaction, the catalyst was heated to 300 °C (heating rate = 3 °C min^{-1}) and reduced with a H_2/N_2 mixture (50 mL min^{-1}, V_{H_2}/V_{N_2} = 1 : 9) for 3 h at atmospheric pressure. The catalyst was then cooled down to 250 °C and the reaction started as gas flow was switched to a H_2/CO mixture (30 mL min^{-1}, $V_{H_2}/V_{CO} = 2 : 1$) at 3 MPa. All post-reactor lines and valves were heated to 150 °C for preventing the possible condensation of products. The products were analyzed for CO, CO_2, alcohols and hydrocarbons on-line by Agilent GC 6820 equipped with a flame ionization detector (FID) and a thermal conductivity detector (TCD). Preliminary experiments with respect to possible influence caused by mass transfer limitation confirmed that such limitation could be ruled out under the reaction conditions used in this work.

The conversion of CO was calculated based on the fraction of CO that formed carbon-containing products according to: % conversion = $(\sum n_i M_i / M_{CO}) \times 100$, where n_i is the number of carbon atoms in product i; M_i is the percentage of product i detected, and M_{CO} is the percentage of CO in the syngas feed. The selectivity of a certain product was calculated based on carbon efficiency using the formula $\%S_i = (n_i C_i / \sum n_i C_i) \times 100$, where n_i and C_i are the carbon number and molar concentration of the product i, respectively. The carbon balance was 100 ± 5%.

2.3. Sample characterization

XRD patterns were recorded on a PANalytical X'Pert instrument using Ni β-filtered Cu K_α radiation (λ = 0.15418 nm) at 40 kV and 40 mA. Two theta angles (2θ) ranged from 10° to 70° with a scanning rate of 4° min^{-1}.

BET specific surface areas (S_{BET}) and pore volumes of the catalysts were measured by N_2 adsorption–desorption isotherms at −196 °C using a Micromeritics ASAP 2020M + C adsorption apparatus after degassing the samples under vacuum at 200 °C for 6 h. S_{BET} was calculated using a value of 0.162 nm^2 for the cross-sectional area of the nitrogen molecule; pore volume was determined by BJH adsorption cumulative volume of pores.

The active copper surface areas (S_{Cu}) in the reduced catalysts were determined by the technique of N_2O reactive frontal chromatography at 60 °C assuming a Cu : N_2O = 2 titration stoichiometry and a surface atomic density of 1.46×10^{19} copper atoms per m^2, respectively.

H_2 temperature-programmed reduction (H_2-TPR) was carried out in a quartz micro-reactor. Firstly, 0.05 g of the prepared catalyst was pre-treated at 300 °C in N_2 for 1 h prior to a TPR measurement. During the TPR experiment, H_2/N_2 mixture gas with $V_{H_2}/V_{N_2} = 1 : 9$ was used at 50 mL min^{-1} and the temperature was ramped from 50 to 500 °C at a rate of 10 °C min^{-1} while the effluent gas was analyzed with a TCD.

CO adsorption properties of the catalysts were studied using a Nicolet 6700 IR spectrometer equipped with a diffuse

reflectance infrared Fourier transform (DRIFT) cell with CaF_2 windows. The sample in the cell was pre-treated in H_2/N_2 (50 mL min^{-1}, $V_{H_2}/V_{N_2} = 1:9$) at 300 °C for 1 h, followed by N_2 (50 mL min^{-1}, Ultrahigh-purity) flushing at 300 °C for 0.5 h. After the temperature was dropped to 30 °C, the background was scanned in N_2 flow. Followed by introducing 0.5% CO/N_2 (50 mL min^{-1}) into the IR cell, the IR spectrum of CO adsorbed on the catalyst was recorded at 30 °C, when adsorption state remained steady. The spectral resolution was 4 cm^{-1} and the number of scans was 64.

Temperature-programmed desorption of adsorbed CO (CO-TPD) was carried out in a quartz micro-reactor. The catalyst (0.1 g) was firstly reduced for 1.5 h at 350 °C in H_2 (50 mL min^{-1}), and then cooled down to 50 °C in He flow. The next step was CO adsorption at 50 °C for 30 min until the surface was saturated. Then the catalyst was swept with He stream for 1 h. Subsequently, the sample was heated in a flowing He stream (50 mL min^{-1}) up to 600 °C at a rate of 10 °C min^{-1}. The desorbed species were detected with a quadrupole mass spectrometer (QMS, Balzers Omnistar 200). MS signals at $m/z = 28$ (CO) and 44 (CO_2) were continuously recorded.

X-ray photoelectron spectra (XPS) experiments were tested on the Thermo Scientific ESCALAB 250Xi spectrometer with an Al anode for Kα (1486.6 eV) radiation. Charging effects were corrected by adjusting the binding energy of C1s peak from carbon contamination to 284.6 eV.

3. Result and discussion

3.1. CO hydrogenation performance of the catalysts

Typical time dependent changes of CO conversion and ROH selectivity on the representative Cu–Fe/SiO_2(WI) catalyst are shown in Fig. 1. It can be seen that both the CO conversion and ROH selectivity changed greatly during the first 10 h on stream, and remained relatively constant after 15 h on stream. Therefore, the data taken at 15–24 h on stream were used as indexes for performance of the catalysts and listed in Table 1. It was found that the orders of the catalysts as to different reactivity parameters are the following:

CO conversion: WI > SR > SI > CC > DP;

ROH selectivity: SI > CC > DP > WI > SR;

CH_x selectivity: SR > CC > WI ≈ SI > DP;

$C_{2+}OH$ selectivity: DP > CC > SI > SR > WI (calculated from ROH selectivity and $C_{2+}OH$ distribution in ROH);

STY of ROH: WI > SI > SR > CC > DP.

Evidently, the performance of the Cu–Fe/SiO_2 catalyst was influenced greatly by its preparation method and the one prepared by ultrasound-assisted wet impregnation showed the highest STY_{ROH} due to the highest CO conversion, which reached 104.3 g kg_{cat}^{-1} h^{-1} and 14.04%, respectively.

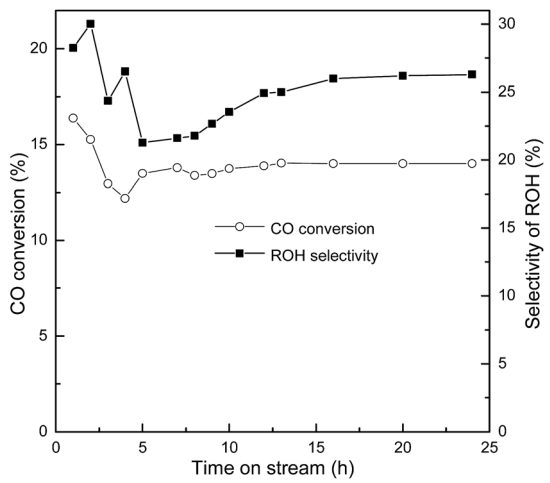

Fig. 1 CO conversion and alcohol selectivity *vs.* time-on-stream on the Cu–Fe/SiO_2(WI) catalyst. Reaction conditions: 250 °C, 3.0 MPa, $V(H_2)/V(CO) = 2$, GHSV = 6000 mL (g h)$^{-1}$.

3.2. Structural and textural properties

Fig. 2 shows the XRD patterns of the different Cu–Fe/SiO_2 catalysts after calcination at 350 °C for 4 h. As shown, the peak at 2θ of 22.5° is attributed to the characteristic diffraction peak of amorphous SiO_2; the peaks at 2θ of 35.6°, 38.8° and 48.7° are attributed to characteristic diffraction peaks of crystal CuO, while that at 2θ of 33.4° can be ascribed to characteristic diffraction peak of α-Fe_2O_3.[20,25] In addition, the peaks at 2θ of 30.1°, 57.0°, and 62.8° are attributed to $CuFe_2O_4$ spinel phase.[11,28]

As shown in Fig. 2, the Cu–Fe/SiO_2(WI) sample only exhibits characteristic diffraction peaks of CuO phase with no Fe_2O_3 phase observable, indicating amorphous nature or the small crystallite size of Fe_2O_3 (less than 5 nm). Neither CuO nor Fe_2O_3 peaks can be clearly observed on Cu–Fe/SiO_2(DP) catalyst, suggesting the crystallite sizes of CuO and Fe_2O_3 are less than 5 nm or the active components are amorphous. The diffraction peaks of CuO over Cu–Fe/SiO_2(SI) sample are sharper than those of the other catalysts, indicating the largest CuO crystallites on Cu–Fe/SiO_2(SI); the crystallite size of CuO calculated by Scherrer equation reaches 20.9 nm (Table 2). In addition, the peak of Fe_2O_3 phase can be clearly observed, indicating the poor dispersion of Fe_2O_3 on Cu–Fe/SiO_2(SI). Compared to Cu–Fe/SiO_2(SI) catalyst, the characteristic diffraction peak of α-Fe_2O_3 disappears and the peaks of CuO are wider on Cu–Fe/SiO_2(SR), indicating the smaller sizes of CuO and Fe_2O_3 on it. As for Cu–Fe/SiO_2(CC), the diffraction peaks of CuO and $CuFe_2O_4$ are clearly observed. The formation of $CuFe_2O_4$ phase can be due to the high combustion temperature.[17]

Specific surface areas and pore volumes of the SiO_2 support and Cu–Fe/SiO_2 catalysts are listed in Table 2. Compared with the support SiO_2, all the Cu–Fe/SiO_2 catalysts show smaller surface areas and pore volumes, which can be attributed to the deposition of oxides of Cu and Fe in pores of SiO_2.[19] Thus, the better dispersion of oxides of Cu and Fe will result in the larger surface area and pore volume of the catalysts. Among the catalysts, Cu–Fe/SiO_2(DP) catalyst shows the largest surface area and pore volume, due to the smallest sizes of oxide particles as evidenced by the result of XRD. Similarly, the smallest surface area of Cu–Fe/SiO_2(SI) is due to the biggest sizes of CuO and Fe_2O_3 particles. Combining the textural

Table 1 Catalytic performance of Cu–Fe/SiO_2 catalysts prepared by different methods in CO hydrogenation[d]

Catalyst code	CO conv. (%)	Selectivity (%)				Alcohol distribution (%)	
		CO_2	CH_x[a]	ROH[b]	STY_{ROH}[c] (g kg_{cat}^{-1} h^{-1})	CH_3OH	$C_{2+}OH$
WI	14.0	18.2	55.0	26.8	104.3	68.4	31.6
DP	5.6	18.1	51.7	30.2	47.0	56.3	43.7
SI	10.2	13.5	54.7	31.8	89.7	65.9	34.1
SR	12.4	16.1	61.9	22.0	75.5	60.6	39.4
CC	7.4	12.2	56.9	31.0	63.3	62.4	37.6

[a] CH_x represents hydrocarbons. [b] ROH represents alcohols. [c] STY_{ROH} represents space time yield of alcohols. [d] Reaction conditions: 250 °C, 3.0 MPa, $V_{H_2}/V_{CO} = 2$, SV = 6000 mL $(g_{cat}\ h)^{-1}$.

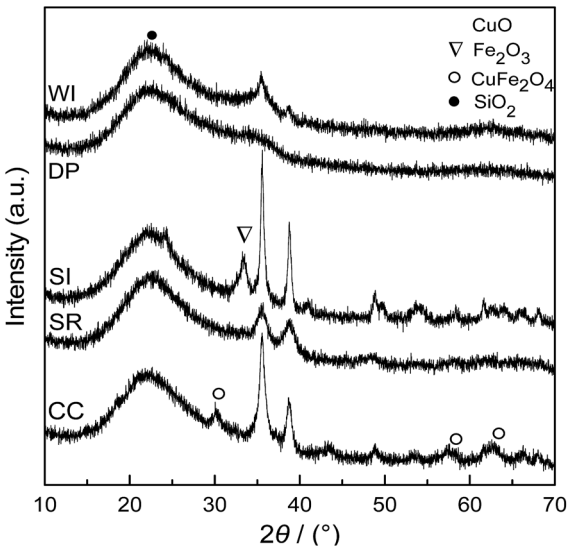

Fig. 2 XRD patterns of Cu–Fe/SiO_2 catalyst prepared by different methods.

parameters (Table 2) and catalytic performance (Table 1) of the catalysts, it can be inferred that the surface area of catalyst is not the main factor affecting the CO conversion and ROH selectivity of the Cu–Fe/SiO_2 catalyst. On the other hand, the higher distribution of $C_{2+}OH$ alcohols of Cu–Fe/SiO_2(DP) and Cu–Fe/SiO_2(SR) can be attributed to the larger pore volume, since the larger pore volume is beneficial to diffusion of reactant molecules in the surface of active site, thereby promoting the formation of long-chain alcohols.[29]

In addition, the active copper surface areas (S_{Cu}) of the Cu–Fe/SiO_2 catalysts after *in situ* reduction are also shown in Table 2. Generally, smaller size of CuO particles contributes to larger active copper surface area. However, the CuO particles may accumulate in the pores of SiO_2, difficult to be reduced by H_2, which leads to the smaller Cu surface area.[26] The combined effects of these two factors account for the difference of S_{Cu} of these Cu–Fe/SiO_2 catalysts. As well known, the catalyst with larger S_{Cu} possesses more active copper species, which is beneficial to the improvement of the activity for hydrogenation. Thus, the order of S_{Cu} (WI > SR > SI = CC > DP) of these Cu–Fe/SiO_2 catalysts is fairly consistent with that of CO conversion (WI > SR > SI > CC > DP). Similar result was also reported by Mahdavi *et al.* who found that the activity of Cu–Co_2O_3/ZnO catalyst increased linearly with S_{Cu}.[30]

3.3. Reducibility of the catalysts

Fig. 3 displays the H_2-TPR profiles of the Cu–Fe/SiO_2 catalysts. For the Cu–Fe/SiO_2(WI) catalyst, two peaks (α and β) could be observed at 213 °C and 230 °C, corresponding to the reduction of highly dispersed and bulk CuO respectively.[16,26] Moreover, the broad peak (γ) detected at 300–500 °C is attributed to the stepwise reduction of Fe_2O_3 ($Fe_2O_3 \rightarrow Fe_3O_4 \rightarrow FeO \rightarrow Fe$).[26,31] Compared with Cu–Fe/SiO_2(WI), the temperature of Fe_2O_3 reduction peak of Cu–Fe/SiO_2(SI) and Cu–Fe/SiO_2(CC) shifts toward higher temperatures, indicating that the reduction of Fe_2O_3 on these two catalysts is more difficult; the reason can respectively be attributed to the larger Fe_2O_3 particles and the formation of $CuFe_2O_4$ (ref. 32) as evidenced by the above XRD result.

Table 2 Physicochemical properties of the SiO_2 support and Cu–Fe/SiO_2 catalysts

Sample	S_{BET}[a] (m^2 g^{-1})	V_p[b] (cm^3 g^{-1})	d_{CuO}[c] (nm)	S_{Cu}[d] (m^2 g^{-1})
SiO_2	261.4	0.89	—	—
Cu–Fe/SiO_2(WI)	203.5	0.53	13.1	4.4
Cu–Fe/SiO_2(DP)	245.9	0.58	—	2.6
Cu–Fe/SiO_2(SI)	192.4	0.54	20.9	3.0
Cu–Fe/SiO_2(SR)	227.9	0.58	9.9	3.2
Cu–Fe/SiO_2(CC)	199.2	0.51	14.1	3.0

[a] The error of S_{BET} is ±1%. [b] The error of V_p is ±2%. [c] Calculated from the CuO(111) peak of the XRD spectra according to the Scherrer equation. [d] Determined by the technique of N_2O reactive frontal chromatography.

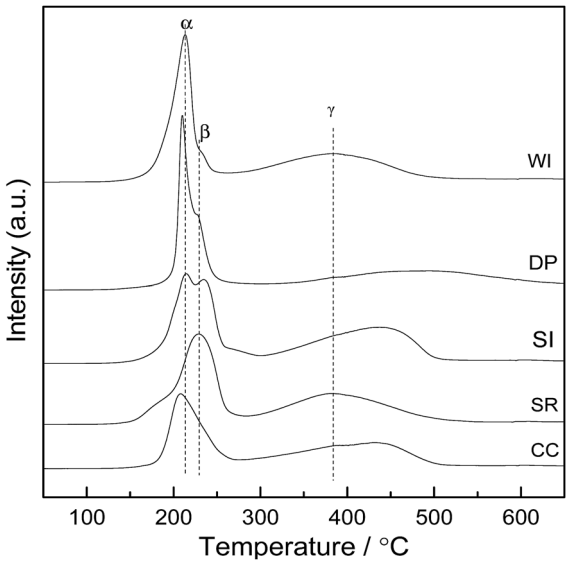

Fig. 3 H_2-TPR curves of the different Cu–Fe/SiO_2 catalysts.

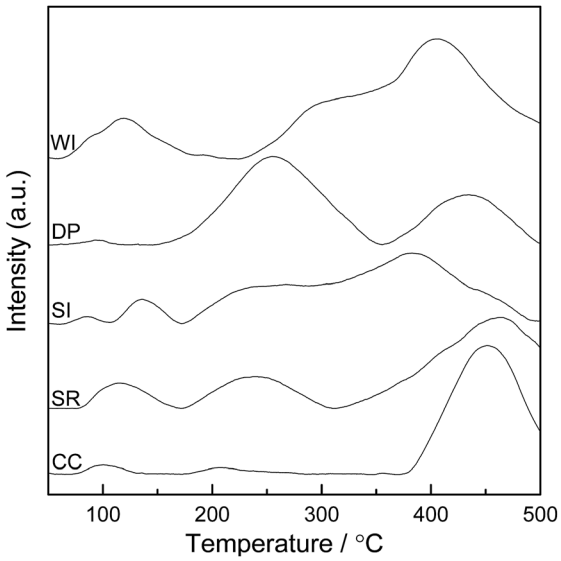

Fig. 4 CO_2-TPD profiles of Cu–Fe/SiO_2 catalyst prepared by different methods.

The peak areas of the reduction peaks of the active constituents are shown in Table 3. The Cu–Fe/SiO_2(DP) and Cu–Fe/SiO_2(CC) catalysts have smaller areas of the reduction peaks of active species compared with the other catalysts, indicating the lower contents of active metals on the surface of catalysts. This is responsible for the lower CO conversion of Cu–Fe/SiO_2(DP) and Cu–Fe/SiO_2(CC).[33]

3.4. CO_2-TPD after CO adsorption

Fig. 4 shows the CO_2-TPD profiles after CO adsorption on the Cu–Fe/SiO_2 catalysts prepared by different methods. Several peaks of CO_2 desorption are found on all the catalysts, indicating that there are several active sites for CO dissociation adsorption. It perhaps took place the CO dissociation or the disproportionation reaction ($2CO \rightarrow C + CO_2$) on the catalyst surface.[34] The peak of CO_2 desorption at low temperature represents the strong active site for CO dissociation adsorption. Therefore, the larger areas of the peaks at low temperature suggest more amounts of strong active sites, thus resulting in higher activity of the catalyst.[35] In this work, the area of CO_2 desorption peak at low temperature (<175 °C) follows the order of WI > SR > SI > CC > DP, which is in good agreement with that of CO conversion as shown in Table 1.

Table 3 The temperatures and areas of reduction peaks for different Cu–Fe/SiO_2 catalysts

	Temperature (°C)			Area (a.u.)	
Catalyst	α	β	γ	α + β	γ
Cu–Fe/SiO_2(WI)	213	230	384	829.4	683.1
Cu–Fe/SiO_2(DP)	210	227	482	727.5	484.6
Cu–Fe/SiO_2(SI)	215	235	432	917.3	771.5
Cu–Fe/SiO_2(SR)	185	230	381	870.2	711.9
Cu–Fe/SiO_2(CC)	208	235	432	615.4	627.6

3.5. Infrared spectra of CO adsorption

IR spectra of CO adsorption on the different Cu–Fe/SiO_2 catalysts are shown in Fig. 5. Apparently, one peak at ~2120 cm^{-1} is observed on Cu–Fe/SiO_2(WI), corresponding to the CO linearly absorbed on copper species.[36] The intensity of the peak increased in the order of DP < SI < CC < SR < WI, which is the same order of CO conversion on them except the catalyst Cu–Fe/SiO_2(CC). The unexpected low activity of the catalyst Cu–Fe/SiO_2(CC) can be attributed to the weak bond of Cu–CO, which can be evidenced by its position at higher wavenumber of 2127 cm^{-1}.[37,38]

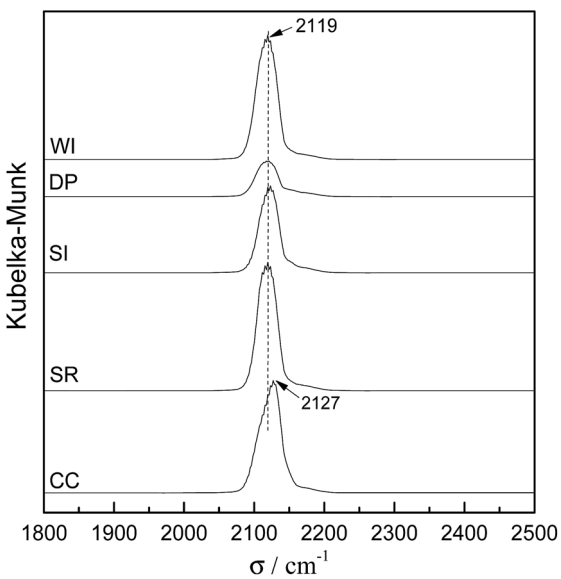

Fig. 5 IR spectra of CO chemisorbed on different Cu–Fe/SiO_2 catalysts.

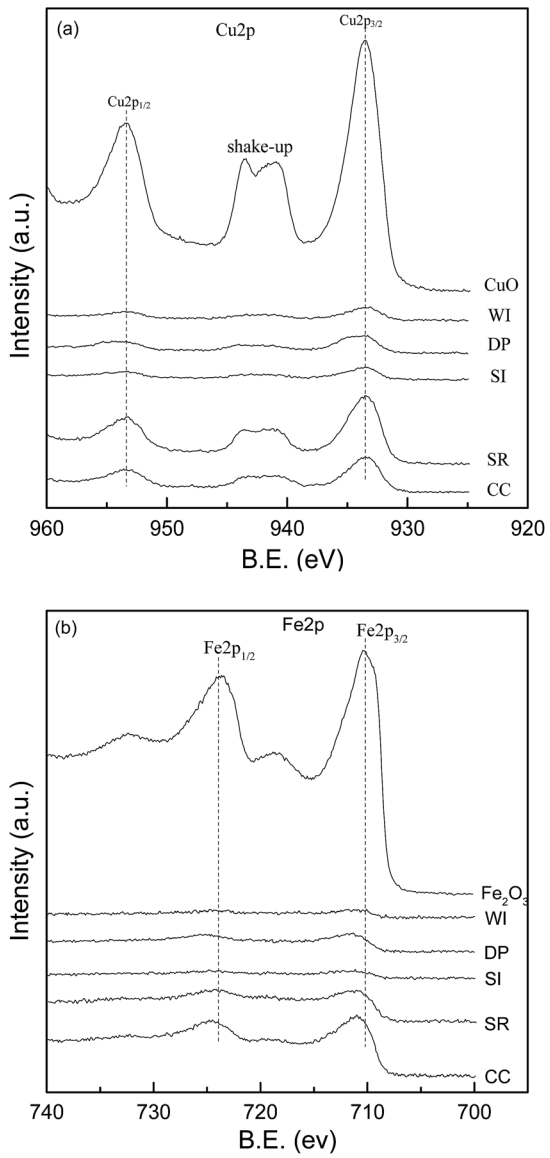

Fig. 6 XPS spectra of the different Cu–Fe/SiO_2 catalysts: (a) Cu2p; (b) Fe2p.

3.6. XPS study

The XPS spectra for Cu2p and Fe2p of CuO, Fe_2O_3 (derived from the decomposition of $Cu(NO_3)_2 \cdot 3H_2O$ and $Fe(NO_3)_3 \cdot 9H_2O$, respectively) and the different Cu–Fe/SiO_2 catalysts are displayed in Fig. 6. For the CuO sample, the $Cu2p_{3/2}$ and $Cu2p_{1/2}$ binding energies at 933.5 and 953.4 eV, could be ascribed to the presence of Cu^{2+} species. For the Fe_2O_3 sample, the $Fe2p_{3/2}$ and $Fe2p_{1/2}$ binding energies at 711.0 and 723.6 eV, could be ascribed to the presence of Fe^{3+}.[21]

The binding energies of $Cu2p_{3/2}$ and $Fe2p_{3/2}$ for the different Cu–Fe/SiO_2 catalysts are summarized in Table 4. It can be seen that the $Cu2p_{3/2}$ binding energy of the Cu–Fe/SiO_2(DP) catalyst is the largest while its $Fe2p_{3/2}$ binding energy is the smallest. This result indicates that the interaction between copper and iron on the Cu–Fe/SiO_2(DP) catalyst is stronger than that on the other catalysts.[16,21] It is well known that the copper has the function of methanol synthesis and the iron element plays an important role in promoting the chain growth. Therefore, the synergism between copper and iron benefits the formation of higher alcohols.[27,28] Accordingly, the strong interaction between copper and iron on the Cu–Fe/SiO_2(DP) catalyst can account for its highest distribution of $C_{2+}OH$ alcohols (Table 1).[39,40]

Table 4 Binding energies of core electrons of the different Cu–Fe/SiO_2 catalysts

	Binding energy (eV)	
Catalyst	$Cu2p_{3/2}$	$Fe2p_{3/2}$
Cu–Fe/SiO_2(WI)	933.3	710.4
Cu–Fe/SiO_2(DP)	934.0	710.1
Cu–Fe/SiO_2(SI)	933.5	711.3
Cu–Fe/SiO_2(SR)	933.4	711.1
Cu–Fe/SiO_2(CC)	933.5	711.0

4. Conclusions

Five Cu–Fe/SiO_2 catalysts were prepared by ultrasound-assisted wet impregnation, deposition–precipitation, solid state impregnation, solid-state chemical reaction, citric acid combustion, and the influence of preparation methods on the physicochemical and catalytic properties for higher alcohols synthesis by CO hydrogenation were investigated. The results indicate that the catalyst prepared by ultrasound-assisted wet impregnation has higher dispersion of active components (Cu, Fe), the maximum of S_{Cu}, higher reducibility, and the strongest CO adsorption capacity and dissociation capability, leading to the highest CO conversion and STY of alcohols.

Acknowledgements

Financial supports provided by the Science and Technology Commission of Shanghai Municipality (13ZR1461900, 08520513600) are gratefully acknowledged.

Notes and references

1 Z. Wang and J. J. Spivey, *Appl. Catal., A*, 2015, **507**, 75.
2 K. G. Fang, D. B. Li, M. G. Lin, M. L. Xiang, W. Wei and Y. H. Sun, *Catal. Today*, 2009, **147**, 133.
3 M. Gupta, M. L. Smith and J. J. Spivey, *ACS Catal.*, 2011, **1**, 641.
4 V. R. Surisetty, A. K. Dalai and J. Kozinski, *Appl. Catal., A*, 2011, **404**, 1.
5 J. J. Spivey and A. Egbebi, *Chem. Soc. Rev.*, 2007, **36**, 1514.
6 V. Subramani and S. K. Gangwal, *Energy Fuels*, 2008, **22**, 814.
7 M. Gupta and J. J. Spivey, *Catal. Today*, 2009, **147**, 126.
8 X. H. Mo, Y. T. Tsai, J. Gao, D. S. Mao and J. G. Goodwin Jr, *J. Catal.*, 2012, **285**, 208.
9 G. Prieto, S. Beijer, M. L. Smith, M. He, Y. Au, Z. Wang, D. A. Bruce, K. P. de Jong, J. J. Spivey and P. E. de Jongh, *Angew. Chem., Int. Ed.*, 2014, **53**, 6397.

10 W. Gao, Y. Zhao, H. Chen, H. Chen, Y. Li, S. He, Y. Zhang, M. Wei, D. G. Evans and X. Duan, *Green Chem.*, 2015, **17**, 1525.
11 K. Xiao, X. Qi, Z. Bao, X. Wang, L. Zhong, K. Fang, M. Lin and Y. Sun, *Catal. Sci. Technol.*, 2013, **3**, 1591.
12 Y. Z. Fang, Y. Liu and L. H. Zhang, *Appl. Catal., A*, 2011, **397**, 183.
13 Y. W. Lu, F. Yu, J. Hu and J. Liu, *Appl. Catal., A*, 2012, **429–430**, 48.
14 M. Lin, K. Fang, D. Li and Y. Sun, *Catal. Commun.*, 2008, **9**, 1869.
15 X. M. Yang, Y. Wei, Y. L. Su and L. P. Zhou, *Fuel Process. Technol.*, 2010, **91**, 1168.
16 H. Zhang, W. Chu, H. Y. Xu and J. Zhou, *Fuel*, 2010, **89**, 3127.
17 D. S. Mao, Q. S. Guo, J. Yu, L. P. Han and G. Z. Lu, *Acta Phys.–Chim. Sin.*, 2011, **27**, 2639.
18 M. Y. Ding, J. G. Liu, Q. Zhang, N. Tsubaki, T. J. Wang and L. L. Ma, *Catal. Commun.*, 2012, **28**, 138.
19 Q. S. Guo, D. S. Mao, J. Yu and L. P. Han, *J. Fuel Chem. Technol.*, 2012, **40**, 1103.
20 J. G. Liu, M. Y. Ding, T. J. Wang and L. L. Ma, *Acta Phys.-Chim. Sin.*, 2012, **28**, 1964.
21 W. Gao, Y. F. Zhao, J. M. Liu, Q. W. Huang, S. He, C. M. Li, J. W. Zhao and M. Wei, *Catal. Sci. Technol.*, 2013, **3**, 1324.
22 Z. H. Bao, K. Xiao, X. Z. Qi, X. X. Wang, L. S. Zhong, K. G. Fang, M. G. Lin and Y. H. Sun, *J. Energy Chem.*, 2013, **22**, 107.
23 J. G. Liu, M. Y. Ding, T. J. Wang and L. L. Ma, *Pet. Process. Petrochem.*, 2013, **44**, 22.
24 S. Kiatphuengporn, M. Chareonpanich and J. Limtrakul, *Chem. Eng. J.*, 2014, **240**, 527.
25 M. Y. Ding, J. L. Tu, J. G. Liu, N. Tsubaki, T. J. Wang and L. L. Ma, *Catal. Today*, 2014, **234**, 278.
26 R. L. Lu, D. S. Mao, J. Yu and Q. S. Guo, *J. Ind. Eng. Chem.*, 2014, **25**, 338.
27 Y. Lu, B. Cao, F. Yu, J. Liu, Z. Bao and J. Gao, *ChemCatChem*, 2014, **6**, 473.
28 H. Guo, H. Zhang, F. Peng, H. Yang, L. Xiong, C. Wang, C. Huang, X. Chen and L. Ma, *Appl. Catal., A*, 2015, **503**, 51.
29 H. Ran, K. Fang, M. Lin and Y. Sun, *Nat. Gas Chem. Ind.*, 2010, **35**, 1.
30 V. Mahdavi, M. H. Peyrovi, M. Islami and J. Y. Mehr, *Appl. Catal., A*, 2005, **281**, 259.
31 C. H. Zhang, Y. Yang, B. T. Teng, T. Z. Li, H. Y. Zheng, H. W. Xiang and Y. W. Li, *J. Catal.*, 2006, **237**, 405.
32 J. Xu and W. Wang, *Chin. J. Catal.*, 1992, **13**, 420.
33 H. Xu, W. Chu, L. Shi, H. Zhang and S. Deng, *J. Fuel Chem. Technol.*, 2009, **37**, 212.
34 C. Mazzocchia, P. Gronchi, A. Kaddouri, E. Tempesti, L. Zanderighi and A. Kiennemann, *J. Mol. Catal. A: Chem.*, 2001, **165**, 219.
35 A. Kiennemann, A. Barama, S. Boujana and M. M. Bettahar, *Appl. Catal., A*, 1993, **99**, 175.
36 R. Xu, Z. Y. Ma, C. Yang, W. Wei, W. H. Li and Y. H. Sun, *J. Mol. Catal. A: Chem.*, 2004, **218**, 133.
37 R. Xu, Z. Y. Ma, C. Yang, W. Wei and Y. H. Sun, *React. Kinet. Catal. Lett.*, 2004, **81**, 91.
38 G. Blyholder and M. Lawless, *Surf. Sci.*, 1993, **290**, 155.
39 R. Xu, C. Yang, W. Wei, W. Li, Y. Sun and T. Hu, *J. Mol. Catal. A: Chem.*, 2004, **221**, 51.
40 R. Xu, W. Wei, W. H. Li, T. D. Hu and Y. H. Sun, *J. Mol. Catal. A: Chem.*, 2005, **234**, 75.